Journal of Power Sources 182 (2008) 61–65

Contents lists available at ScienceDirect

Journal of Power Sources

journal homepage: www.elsevier.com/locate/jpowsour

Optimization of the performance of polymer electrolyte fuel cell membrane-electrode assemblies: Roles of curing parameters on the catalyst and ionomer structures and morphology

Anima B. Bose[a,*], Ruhulla Shaik[a], Jennifer Mawdsley[b]

[a] Department of Mechanical Engineering, Northern Illinois University, DeKalb, IL 60115, USA
[b] Chemical Sciences and Engineering Division, Argonne National Laboratory, 9700 S. Cass Avenue, Argonne, IL 60439, USA

ARTICLE INFO

Article history:
Received 7 February 2008
Received in revised form 20 March 2008
Accepted 21 March 2008
Available online 11 April 2008

Keywords:
PEM fuel cells
Membrane-electrode assembly fabrication
Electrode morphology
Ionomer dynamics
Scanning electron microscopy

ABSTRACT

In order to understand the origin of performance variations in polymer electrolyte membrane fuel cells (PEMFCs), a series of membrane-electrode assemblies (MEAs) with identical electrode layer compositions were prepared using different electrode curing conditions, their performances were evaluated, and their morphologies determined by scanning electron microscopy (SEM). The polarization curves varied markedly primarily due to differences in morphologies of electrodes, which were dictated by the curing processes. The highest performing MEAs (1.46 W cm^{-2} peak power density at 3.2 A cm^{-2} and 80 °C) were prepared using a slow curing process at a lower temperature, whereas those MEAs prepared using a faster curing process performed poorly (0.1948 W cm^{-2} peak power density at 440 mA cm^{-2} and 80 °C). The slowly cured MEAs showed uniform electrode catalyst and ionomer distributions, as revealed in SEM images and elemental maps. The relatively faster cured materials exhibited uneven distribution of ionomer with significant catalyst clustering. Collectively, these results indicate that to achieve optimal performance, factors that affect the dynamics of the curing process, such as rate of solvent evaporation, must be carefully controlled to avoid solvent trapping, minimize catalyst coagulation, and promote even distribution of ionomer.

1. Introduction

In recent years, a great deal of interest has been focused on preparing materials and fabricating high performing and durable membrane electrode assemblies (MEAs) for polymer electrolyte membrane fuel cells (PEMFCs) and direct methanol fuel cells (DMFCs) [1,2]. Among many issues, preparation of durable catalysts, lowering platinum loadings and increasing platinum utilization [3–7], and creation of robust membranes operating above 80 °C and at low relative humidity [8,9] have been given utmost priority. Particular attention has been given to stabilizing the catalyst particles in the electrode layers and to the morphological and structural properties of electrode on cell performance [3–5,7,10–12]. The stabilization and distribution of the ionomer in the electrode layer also affects the performance of PEMFCs and DMFCs. This ionomer is typically Nafion®, a perfluorosulfonic acid polymer, chosen for its excellent interfacial compatibility with the membrane material, which is also Nafion®, its chemical stability, high proton conductivity, and high oxygen solubility [13]. Nafion® content in the active catalyst layer largely influences the performance of electrodes of MEAs by influencing the gas permeability, ionic resistance, and catalyst utilization [3,14–19]. Significant improvements in PEMFC performance have been reported when a gradient composition of Nafion® in the range of 25–40 wt%, with higher contents towards the bulk electrolyte, was used as compared to uniform distribution of ionomer throughout the catalyst layer [14,16].

Three commonly used methods to prepare MEAs are: (1) painting an ionomer-catalyst ink onto the gas diffusion layer [14,18,20–22], (2) applying the ink directly onto the membrane [2,3,15,23,24], or (3) transferring the dried catalyst ink onto the membrane by hot-pressing a catalyst ink decal [13,25] Many approaches have been reported for ink preparation and MEA fabrication that result in improved performance and durability [2,19,26]. A common practice of ink preparation includes physical dispersion of the Pt/C catalyst into a polymeric Nafion® solution. Alternatively, graft polymerization of perfluorosulfonated monomers has been directly initiated in the Pt/C mixtures to generate a uniform platinum-electrolyte interface in the electrode [4]. This technique has afforded uniform pore distributions with pore sizes in the range 0.02–0.06 μm, and uniform growth of polymer electrolyte

* Corresponding author. Tel.: +1 815 753 8024; fax: +1 815 753 0416.
E-mail address: bose@ceet.niu.edu (A.B. Bose).

0378-7753/$ – see front matter © 2008 Published by Elsevier B.V.
doi:10.1016/j.jpowsour.2008.03.070

on the carbon surface, thereby increasing the electrochemically active surface area [4]. Even within the constraints of uniformity described above, there are examples of variation in MEA performance occurring for identical MEA compositions [27]. In order to understand such variations in performance, several investigators have emphasized the roles of structures and morphologies of catalysts [3,19,28–32]. Although non-uniformity of impregnated Nafion® in the catalyst layer [23] and localization of Nafion® on the external surface of the electrode [33] have been observed, the reasons for such formations are poorly understood. It is clear that limited attention has been given to the dynamics of the fabrication processes which, due to its influence on microstructures and morphologies, likely affects performance.

Here, we address some key factors that control the performance of MEAs fabricated using standard materials: Pt/C catalyst, Nafion® ionomer, and Nafion® membrane electrolyte. In particular, we have prepared several sets of MEAs and three such sets with almost identical compositions using different curing conditions, measured their performances, determined their structural features by SEM and EDX, and correlated that with the observed performance. The present study clearly demonstrates how the dynamics of the electrode curing process of the catalyst-ionomer ink controls the morphology, distribution, and structure of both the electrocatalyst and the ionomer and hence influences the performance of MEAs.

2. Experimental procedures

2.1. MEA fabrication

MEAs with 5 cm^2 active area were prepared by depositing 40 wt% Pt/C (Alfa Aesar) catalyst mixed with Nafion® onto homemade Nafion® membranes that were prepared using 5 wt% Nafion® solution (DE 521, DuPont). Several sets of MEAs were prepared using the same batch of in-house prepared membrane, but results of two sets abbreviated as MEA-1 and MEA-2, are presented in the results section. The third set of MEAs (MEA-3) was fabricated from a separate batch of in-house prepared membrane. The in-house membranes were prepared using the following procedure. First, the membranes were cast using a 5% Nafion® solution, and then boiled in 3 M H_2O_2 for an hour, followed by a boiling in 5% H_2SO_4 for an hour. Finally, the membranes were boiled in de-ionized water for an hour to remove excess acid. The thicknesses of the membranes are 30 μm for MEA-1 and MEA-2, and 20 μm for MEA-3. The application of the electrode inks was identical within the experimental error; however, the curing conditions were different as described below.

The MEAs were prepared by direct deposition of the catalyst ink onto the membranes using a spray gun (Badger Airbrush: 155-1). The ink was deposited onto both sides of the membrane with anode and cathode catalyst loadings of 0.25 mg Pt cm^{-2} and 0.50 mg Pt cm^{-2}, respectively. The catalyst loadings were maintained at the same level for all three MEAs and the same catalyst-ionomer ink batch was used for all three MEAs as well. The ratio of Pt/C catalyst to Nafion® solution used in the ink resulted in electrodes with 30 wt% ionomer content. The catalyst-ionomer ink was prepared by mixing 3 mL of deionized water with 0.5 g of 40 wt% Pt/C in an ultrasonic bath for one minute. Seven milliliters of isopropyl alcohol was then mixed with the solution, followed by mixing in the 5 wt% Nafion® solution at 30 wt% with respect to the Pt/C. Lastly, the solution was left to stir for 24 h before use. After spraying the ink onto the membranes, the solvent was evaporated in a controlled manner under an IR-lamp. The curing conditions were varied by (1) changing the distance between the MEA and the IR lamp, resulting in different MEA temperatures and (2) changing the amount of time between two consecutive sprays. During the catalyst deposition for MEA-1 and MEA-3, the solvent evaporation time was 8–10 min between two consecutive sprays. After each spray, the catalyst layer was dried under the IR lamp at a temperature of ~50 °C. The solvent evaporation time between the two consecutive sprays of catalyst ink onto MEA-2 was reduced to 5 min and the drying temperature was increased to ~60 °C by reducing the distance between the IR lamp and the MEA. After spraying the ink on both sides of the membrane to deposit the designated amounts of Pt/C for the anode and cathode, the MEAs were hot-pressed at 120 °C for 10 min under 1000 pounds of pressure (Carver 3853-0 Model C).

2.2. MEA evaluation and characterization

The performance measurements of all MEAs were conducted at 60 °C and 80 °C using a flow rate of 0.2 L min^{-1} for both H_2 and O_2 with an operating pressure of 30 psi, and with both gases humidified to 100% relative humidity using a Fuel Cell Test Station 890CL (Scribner Associates Inc.). For the cathode electrochemically-active surface area (ECSA) measurements, a typical half-cell configuration was used by passing nitrogen at the cathode and hydrogen at the anode. The ECSA measurements were made between 0 and 0.8 V using Corrware software (Scribner Associates Inc.) and an SI 1287 (Solatron Analytical) potentiostat at scan rate 30 mV s^{-1}. The ECSAs were calculated using the charge generated from hydrogen adsorption/desorption and the well-known charge for hydrogen adsorption of 210 μC cm^{-2}-Pt [34,35].

One common practice of preparing MEAs for SEM investigation is to cut the MEAs after freezing them in liquid nitrogen [36,37]. However, elemental mapping by energy dispersive X-ray spectroscopy (EDX) requires a surface that is polished flat in order to achieve results with the highest reliability [38]. For our SEM investigation, a piece from each MEA was cast in a polyester resin (Castolite, LECO Corp.) and polished using standard polishing techniques for polymers and plastics [38]. The samples were oriented such that a cross-sectional view of the MEAs was revealed. The samples were then examined in an SEM (JEOL JSM-6400) using energy dispersive X-ray spectroscopy (EDX, Oxford) for elemental mapping.

3. Results and discussion

A number of MEAs with identical catalyst and ionomer compositions were prepared under different curing conditions and their performances were evaluated. Three such MEAs representing two extremes in performance will be discussed in detail. Figs. 1–3 show

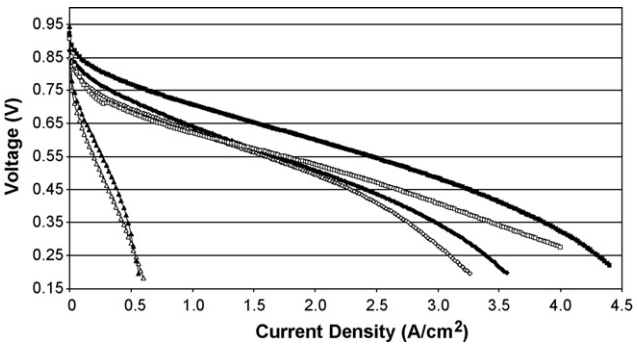

Fig. 1. Non-IR free performance curves of MEA-1, MEA-2, and MEA-3 at 60 °C and 80 °C operated on H_2/O_2 at 60/60/60 °C and 80/80/80 °C of $T_{cell}/T_{cathode\ humidity}/T_{anode\ humidity}$. (●) MEA-1 at 80 °C; (■) MEA-2 at 80 °C; (▲) MEA-3 at 80 °C (hollow symbols represent 60 °C performances).

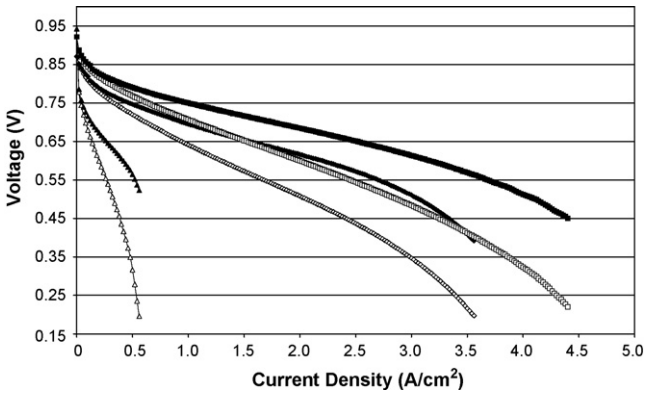

Fig. 2. Polarization (IR free and non-IR free) curves of MEA-1, MEA-2 and MEA-3 operated on H_2/O_2 at 80/80/80 °C of $T_{cell}/T_{cat\ humidity}/T_{anode\ humidity}$. (●) MEA-1 at 80 °C; (■) MEA-2 at 80 °C; (▲) MEA-3 at 80 °C (hollow symbols represent non-IR free performances at 80 °C).

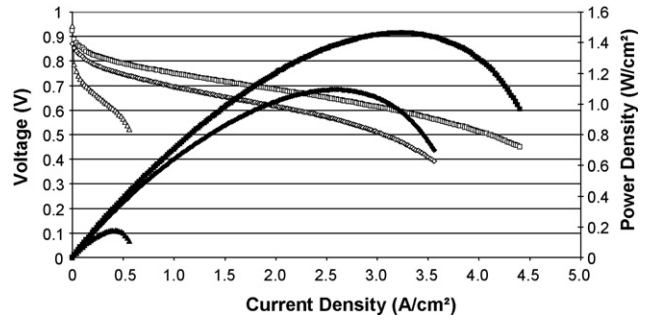

Fig. 3. Performance and power density curves of MEA-1, MEA-2, and MEA-3 operated on H_2/O_2 at 80/80/80 °C of $T_{cell}/T_{cat\ humidity}/T_{anode\ at\ 100\%\ RH}$. (●) Power of MEA-1 at 80 °C; (■) power of MEA-2 at 80 °C; (▲) power of MEA-3 at 80 °C (hollow symbols represent the performance).

typical polarization curves, taken at 60 °C and 80 °C, for the three MEAs. A summary of the performance data at both 60 °C and 80 °C is given in Table 1. As can be seen from the Fig. 3 and Table 1, the peak power densities for the best performing MEA, MEA-3, at 60 °C and 80 °C were observed to be 1.226 W cm^{-2} and 1.462 W cm^{-2}, respectively. Similarly, the current densities at these temperatures were 0.4 A cm^{-2} and 1.06 A cm^{-2}, respectively, at a potential of 0.7 V. The current and power densities for MEA-1 and MEA-3 approach those reported in the literature for similar test conditions [39].

The distinct difference between the three MEAs was the conditions under which they were cured. This difference in the conditions of the curing process led to a wide variation in performance. These conditions include variation in drying temperature and time between the consecutive sprays during the curing process. In MEA-1, a slow electrode drying process yielded 1.104 W cm^{-2} peak power density at 2.78 A cm^{-2} and 80 °C. Whereas for MEA-2, fabricated using a faster electrode curing process afforded only 0.1948 W cm^{-2} peak power density at 0.44 A cm^{-2} and 80 °C. Likewise, MEA-1 exhibits a current density of 0.46 A cm^{-2} at 0.7 V compared to 80 mA cm^{-2} for MEA-2 at the same potential. MEA-3, which was prepared using a slow curing process like that of MEA-1, exhibited a peak power density of 1.464 W cm^{-2} at 80 °C. The higher performance of MEA-3 compared to MEA-1 is due to a thinner membrane (20 μm for MEA-3 as compared to 30 μm for MEA-1). It is known that cells containing Nafion® perform better at 80 °C than at 60 °C [8], which was observed for both MEA-1 and MEA-3, as shown in Table 1. However, MEA-2 did not show any improvement in cell performance by raising the temperature from 60 °C to 80 °C, which implies that the performance was not limited by a temperature-dependent process, such as proton conduction, but by a relatively temperature-independent process, such as reactant mass transfer. Since MEA-3 had a different membrane thickness than the other MEAs, we will focus the remainder of our analysis on the other two MEAs, MEA-1 and MEA-2, which had identical membrane thicknesses.

To fully understand the large difference in performance between MEA-1 and MEA-2, which had identical compositions, detailed electrochemical and morphological analyses were performed. To determine the source of the cell resistance among all possible sources of resistance (activation, ohmic, and mass transport) responsible for the differences in performance, the ohmic resistances of MEA-1, MEA-2, and MEA-3 were determined (Table 1) by the current interrupt technique. This ohmic resistance was used to determine the IR-free performances of these three MEAs (Fig. 2). As can be seen from Fig. 2, there is contribution from mass transfer resistance only at the higher current densities, above 2 A cm^{-2}, for the better-performing MEA's, MEA-1 and MEA-3. However, after IR correction, MEA-2 showed significant signs of activation losses and of mass transfer losses at virtually all current densities.

Cyclic voltammograms (CVs) of the cathodes were collected in order to compare the electrochemically-active surface areas (ECSA) of the platinum electrocatalysts. The half-cell CVs were obtained in the potential range of 0–0.8 V at a scan rate of 30 mV s^{-1}. The calculated ECSAs, assuming a total platinum loading of 2.5 mg, in MEA-1 and MEA-2 were 34.9 m^2 g^{-1}-Pt and 32.9 m^2 g^{-1}-Pt, respectively. These calculations show that these two MEAs have comparable ECSAs and that the differences in the performances of these two MEAs cannot be attributed to differences in the amount of cathode catalyst surface area in contact with both an electronic and ionic conductor.

Table 1
Comparison of MEA-1, MEA-2, and MEA-3 at 60 °C and 80 °C

Measurement	Temperature (°C)	MEA-1	MEA-2	MEA-3
OCP (V)	60	0.831	0.922	0.906
	80	0.846	0.943	0.920
ECSA (m^2 g^{-1}-Pt)		34.9	32.9	36.7
ECSA (cm^2-Pt cm^{-2}-electrode)		174	165	183
Current density at 0.7 V (A cm^{-2})	60	0.460	0.040	0.400
	80	0.620	0.080	1.060
Peak power density (W cm^{-2})	60	1.094	0.152	1.226
	80	1.032	0.175	1.464
Current density at peak power (A cm^{-2})	60	2.640	0.440	3.060
	80	2.420	0.420	3.240
High frequency area-specific resistance (Ω cm^2)	60	0.094	0.162	0.094
	80	0.091	0.159	0.089

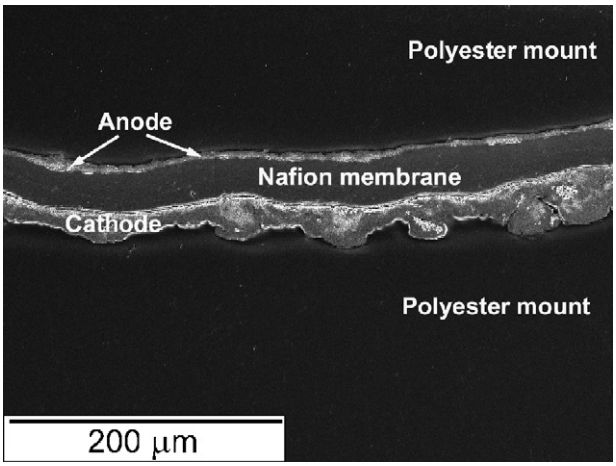

Fig. 4. SEM image of MEA-2 cross-section showing large variations in the thickness of the cathode.

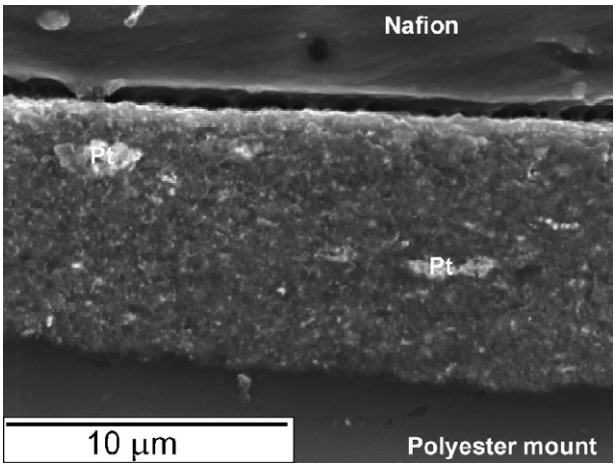

Fig. 6. SEM image of MEA-1 cathode cross-section. A few small Pt agglomerates can be seen.

To understand the performance variations, SEM images and EDX elemental maps were acquired to reveal the morphology and structure of the catalyst layer, examples of which are shown in Figs. 4–7. There were distinct differences between MEA-1 and MEA-2. The cathode of MEA-2, shown in Fig. 4, clearly has a non-uniform thickness. The outer surface of the cathode of MEA-2, which was in contact with the gas diffusion layer during the electrochemical tests, clearly has an uncommonly high surface roughness. A higher magnification image of the cathode of MEA-2 can be seen in Fig. 5a–c show EDX elemental maps of the Pt and F, respectively, for a selected area of Fig. 5a. In the Pt map shown in Fig. 5b, it can be seen that in MEA-2 there was regional clustering of Pt and the fluorine map in Fig. 5c revealed uneven distributions of Nafion® as evidenced by the presence of several bright areas of the order of 10 μm in dimension that correspond to higher concentrations of fluorine along with several dark areas in the map that have lower fluorine concentrations. In contrast, SEM images of MEA-1 showed very few areas of Pt clustering, as seen in Fig. 6. In these few clustered areas, catalyst agglomerations appeared to be much smaller. Also, the light and dark areas in the cathode of MEA-1 cor-

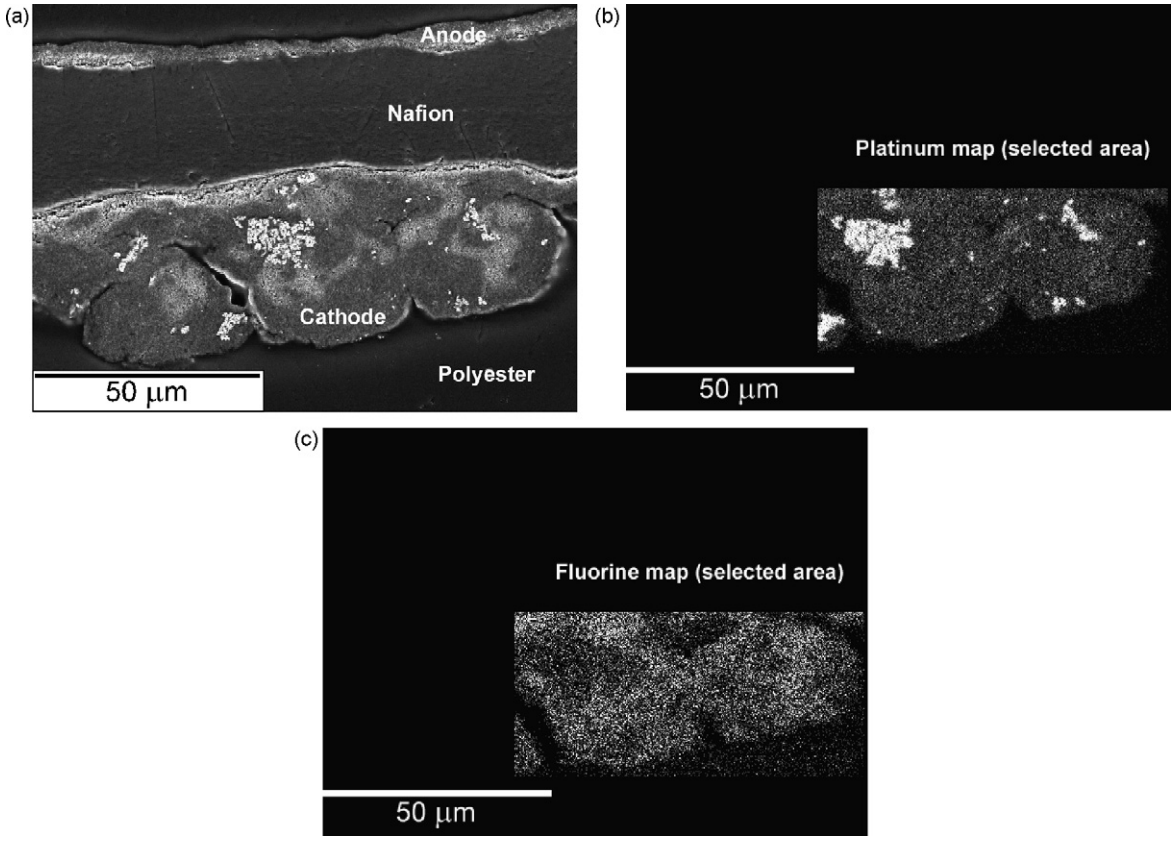

Fig. 5. (a) SEM image of MEA-2 cathode cross-section. (b) EDX platinum map of MEA-2 cathode for a selected area of (a). (c) EDX fluorine map of MEA-2 for a selected area of (a).

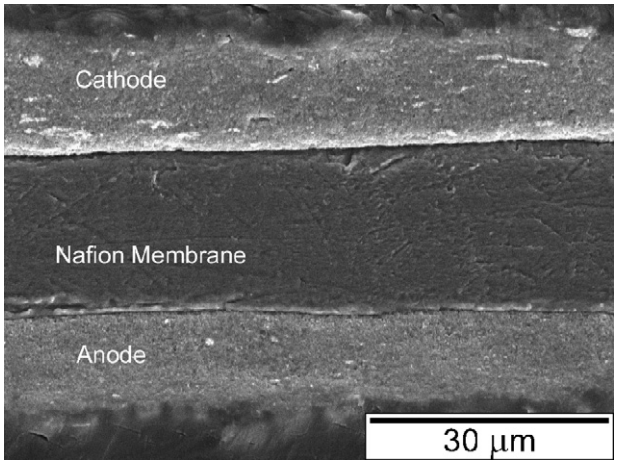

Fig. 7. SEM image of MEA-3 cross-section.

responding to fluorine are about 0.5 μm in diameter and evenly distributed through the electrode creating a more homogenous structure. MEA-3, shown in Fig. 7, also exhibits a catalyst morphology and homogeneous Nafion® distribution very much identical to that of MEA-1. Taking the images shown in Figs. 4–7 collectively, it is quite clear that the distribution of Nafion® ionomer within the cathode of MEA-2 is extremely inhomogeneous in nature, compared to MEA-1 and MEA-3.

The SEM images discussed above provide a clear correlation between performance and electrode structures for MEA-1 and MEA-2, which had identical electrode compositions and membrane thicknesses. The poor performance of MEA-2 compared to MEA-1 is likely a result of the undesired localization of the ionomer. While MEA-1 and MEA-2 have nearly identical ECSAs, indicating that the catalyst utilization is identical for the two, despite the apparent clustering of the Pt in MEA-2, the distribution of the Nafion® ionomer is not the same, as shown in Fig. 5c. An ideal electrode microstructure would have the ionomer well dispersed in order to create the maximum number of triple phase boundaries between the Pt/C, ionomer, and gas pores [40]. In the case of MEA-2 there are areas that are ionomer poorly distributed, thus we expect that there are fewer triple phase boundaries in those regions, which results in poor performance. Additionally, the areas that have high concentrations of ionomer may have blocked gas flow paths which could lower the performance of the MEA as well.

4. Conclusions

The results presented above show that the performance of our MEAs largely depended on the curing processes, which controlled the catalyst and ionomer distributions. A lower curing temperature allowed for slow solvent evaporation in the electrode layer, eliminated solvent trapping, and resulted in uniform dispersion of ionomer and catalyst. The performance of MEAs fabricated using the slow curing process was relatively high. A faster curing process, achieved by increasing the curing temperature, resulted in catalyst coagulations, ionomer clustering, and uneven distributions of the catalyst and ionomer. This in turn led to poor MEA performance compared to MEAs cured slowly.

Acknowledgements

Funding of this research by the U.S. Department of Transportation to Northern Illinois University is gratefully acknowledged. We thank Dr. P. Vohra, for his support and Mr. P. Babburi technical assistance.

References

[1] H.A. Gasteiger, S.S. Kocha, B. Sompalli, F.T. Wagner, Appl. Catal. B: Environ. 56 (1-2) (2005) 9–35.
[2] H. Xu, Y. Song, H.R. Kunz, J.M. Fenton, J. Electrochem. Soc. 152 (9) (2005) A1828–A1836.
[3] X.L. Cheng, B.L. Yi, M. Han, J.X. Zhang, Y.G. Qiao, J.R. Yu, J. Power Sources 79 (1) (1999) 75–81.
[4] H. Mizuhata, S. Nakao, T. Yamaguchi, J. Power Sources 138 (1-2) (2004) 25–30.
[5] M. Uchida, Y. Fukuoka, Y. Sugawara, N. Eda, A. Ohta, J. Electrochem. Soc. 143 (7) (1996) 2245–2252.
[6] N.P. Ugarte, K.E. Swider-Lyons, Proton Conducting Membrane Fuel Cells III Proceedings, 2005, pp. 67–73.
[7] K. Wikander, H. Ekstroem, A.E.C. Palmqvist, G. Lindbergh, Electrochim. Acta 52 (24) (2007) 6848–6855.
[8] M.V. Williams, H.R. Kunz, J.M. Fenton, J. Power Sources 135 (1-2) (2004) 122–134.
[9] S.M.J. Zaidi, S.U. Rahman, J. Electrochem. Soc. 152 (8) (2005) A1590–A1594.
[10] S. Ball, S. Hudson, B. Theobald, D. Thompsett, ECS Trans. 1 (8) (2005) 141–152.
[11] S. Koh, J. Leisch, M.F. Toney, P. Strasser, J. Phys. Chem. C 111 (9) (2007) 3744–3752.
[12] B.N. Popov, H.R. Colon-Mercado, J. Power Sources 155 (2) (2006) 253–263.
[13] M.S. Wilson, S. Gottesfeld, J. Electrochem. Soc. 139 (2) (1992) L28–L30.
[14] P. Gode, F. Jaouen, G. Lindbergh, A. Lundblad, G. Sundholm, Electrochim. Acta 48 (28) (2003) 4175–4187.
[15] S. Hirano, J. Kim, S. Srinivasan, Electrochim. Acta 42 (10) (1997) 1587–1593.
[16] E. Passalacqua, F. Lufrano, G. Squadrito, A. Patti, L. Giorgi, Electrochim. Acta 46 (6) (2001) 799–805.
[17] G. Sasikumar, J.W. Ihm, H. Ryu, J. Power Sources 132 (1-2) (2004) 11–17.
[18] D.T. Song, Q.P. Wang, Z.S. Liu, M. Eikerling, Z. Xie, T. Navessin, S. Holdcroft, Electrochim. Acta 50 (16-17) (2005) 3347–3358.
[19] E.A. Ticianelli, C.R. Derouin, S. Srinivasan, J. Electroanal. Chem. 251 (2) (1988) 275–295.
[20] G.C. Li, P.G. Pickup, J. Electrochem. Soc. 150 (11) (2003) C745–C752.
[21] V.A. Paganin, E.A. Ticianelli, E.R. Gonzalez, J. Appl. Electrochem. 26 (3) (1996) 297–304.
[22] R.R. Passos, V.A. Paganin, E.A. Ticianelli, Electrochim. Acta 51 (25) (2006) 5239–5245.
[23] M.S. Wilson, S. Gottesfeld, J. Appl. Electrochem. 22 (1) (1992) 1–7.
[24] J. Xie, F. Garzon, T. Zawodzinski, W. Smith, J. Electrochem. Soc. 151 (7) (2004) A1084–A1093.
[25] M.S. Wilson, J.A. Valerio, S. Gottesfeld, Electrochim. Acta 40 (3) (1995) 355–363.
[26] O.J. Murphy, G.D. Hitchens, D.J. Manko, J. Power Sources 47 (3) (1994) 353–368.
[27] D. Liu, S. Case, J. Power Sources 162 (1) (2006) 521–531.
[28] D.S. Chan, C.C. Wan, J. Power Sources 50 (3) (1994) 261–281.
[29] N. Giordano, E. Passalacqua, V. Alderucci, P. Staiti, L. Pino, H. Mirzaian, E.J. Taylor, G. Wilemski, Electrochim. Acta 36 (5-6) (1991) 1049–1055.
[30] N. Giordano, E. Passalacqua, V. Recupero, M. Vivaldi, E.J. Taylor, G. Wilemski, Electrochim. Acta 35 (9) (1990) 1411–1421.
[31] M. Watanabe, K. Makita, H. Usami, S. Motoo, J. Electroanal. Chem. 197 (1-2) (1986) 195–208.
[32] M. Watanabe, M. Tomikawa, S. Motoo, J. Electroanal. Chem. 195 (1) (1985) 81–93.
[33] Z. Poltarzewski, P. Staiti, V. Alderucci, W. Wieczorek, N. Giordano, J. Electrochem. Soc. 139 (3) (1992) 761–765.
[34] I. Avila-Garcia, M. Plata-Torres, M.A. Dominguez-Crespo, C. Ramirez-Rodriguez, E.M. Arce-Estrada, J. Alloys Compd. 434–435 (2007) 764–767.
[35] S. Trasatti, O.A. Petrii, Pure Appl. Chem. 63 (5) (1991) 711–734.
[36] N.P. Siegel, M.W. Ellis, D.J. Nelson, M.R. von Spakovsky, J. Power Sources 115 (1) (2003) 81–89.
[37] J. Xie, D.L. Wood, D.M. Wayne, T.A. Zawodzinski, P. Atanassov, R.L. Borup, J. Electrochem. Soc. 152 (1) (2005) A104–A113.
[38] L.C. Sawyer, D.T. Grubb, Polymer Microscopy, Chapman & Hall, London, 1996, pp. 91–94.
[39] H.A. Gasteiger, W. Gu, R. Makharia, M.F. Mathias, B. Sompalli, in: W. Vielstich, A. Lamm, H.A. Gasteiger (Eds.), Handbook of Fuel Cells—Fundamentals, Technology, and Applications, John Wiley & Sons, Ltd., West Sussex, England, 2003, pp. 591–610.
[40] R. O'Hayre, D.M. Barnett, F.B. Prinz, J. Electrochem. Soc. 152 (2) (2005) A439–A444.